

Generation of a Schrödinger cat state in a hybrid ferromagnet-superconductor system

Shiwen He¹,^{*} Xuanxuan Xin,¹ Feng-Yang Zhang,^{2,*} and Chong Li^{1,†}

¹*School of Physics, Dalian University of Technology, Dalian 116024, China*

²*School of Physics and Materials Engineering, Dalian Minzu University, Dalian 116600, China*



(Received 24 August 2022; accepted 30 January 2023; published 13 February 2023)

The hybrid system between the transmon and the magnon plays an important role in quantum information science. Additionally, the cat states of the magnon are a valuable quantum resource and represent macroscopic quantum superpositions of large numbers of spins. In this paper, we propose an approach to generate magnonic Schrödinger cat states (SCSs) in a hybrid ferromagnet-superconductor system. Moreover, high-fidelity magnonic SCSs can be generated when the dissipation of the system is considered. The coherent amplitude and the fidelities of the cat states can be adjusted by controlling the parameters of the system.

DOI: [10.1103/PhysRevA.107.023709](https://doi.org/10.1103/PhysRevA.107.023709)

I. INTRODUCTION

Hybrid systems incorporate advantages from various physical systems, causing them to play a crucial role in quantum information processing [1–3]. With the rapid development of quantum technologies, a lot of attention has been focused on hybrid quantum systems consisting of magnons and superconducting qubits. Both magnons and superconducting qubits have their unique characteristics. For example, superconducting qubits can easily be expanded and manipulated [4–8]. Superconducting qubits are “artificial atoms” based on mesoscopic circuits with multiple discrete energy levels. They are characterized by controllability, scalability, and interface capabilities [4,5,9–14]. Anharmonicity of the superconducting qubit allows quantification into an effective two-level model. On the other hand, ferromagnetic material samples of spin collective excitation, such as yttrium iron garnet (YIG) spheres, can be called magnons. These magnons have a high spin density, long lifetimes, and low dissipation [15–20], and they can interact coherently with optical photons, microwaves, and phonons [21] through magneto-optical [22–30], magnetic dipole [15–17,20,31–39], and magnetostrictive interactions [29,40], respectively. Magnons are ideal candidates for the study of macroscopic quantum effects. In addition, the Kittel mode is the most basic mode of the magnon. An ensemble of spins in a uniformly saturated and magnetized YIG sphere can be considered a macroscopic spin [20].

In a ferromagnetic superconducting qubit hybrid system, the magnon mode and the superconducting qubit can be strongly coupled to the microwave cavity field when they are resonant with it. In contrast, the direct interaction between the magnon and superconducting qubit is so weak as to be negligible. With the development of a hybrid system, coherent coupling between a YIG sphere and a transmon-type [7] superconducting qubit has been experimentally demonstrated

recently [13]. A YIG sphere in the Kittel mode and a two-level superconducting qubit are mounted in a copper microwave cavity. The YIG sphere is excited by an external local static magnetic field B_{basis} along the z axis, which can be employed to modulate the frequency of the magnon. Both the superconducting qubit and the magnon frequencies are tuned to far-detuned frequencies compared to the cavity frequency in a static coupling scheme between the superconducting qubit and the magnon. Coherent coupling between the magnon and the superconducting qubit is achieved under a near-resonant condition. The virtual-photon excitation in the cavity mode mediates the coherent exchange between the superconducting qubit and the magnon [13]. Therefore, quantum states can convey coherently from the superconducting qubit to the magnon. Hybrid quantum systems with magnons have become a suitable platform for new quantum technologies in recent years. For example, such a system has been implemented in the quantum control of a single magnon [41], entangled-state generation [42], and magnon blockades [43,44].

Schrödinger initially introduced a superposition of dead and alive cat states, which is known as the Schrödinger cat state (SCS) [45]. A living cat is macroscopically distinguishable from a dead cat. A coherent state is considered a quasiclassical state with minimal uncertainties and therefore SCSs are defined as the quantum superposition of separate quasiclassical states [46–50]. SCSs have a normal form as $\mathcal{N}(|\alpha\rangle \pm |-\alpha\rangle)$, where \mathcal{N} is the normalization coefficient; $|\alpha\rangle$ denotes a coherent state; $|\alpha\rangle + |-\alpha\rangle$ and $|\alpha\rangle - |-\alpha\rangle$ are respectively the Schrödinger even cat state (SECS) with even number distributions and the Schrödinger odd cat state (SOCS) with odd number distributions. SCSs not only serve as fundamental tests of quantum theory [51–54] but also are applied as a tool for research in understanding the transition between the microscopic and macroscopic worlds in quantum measurement theory [55,56]. Schemes for the generation of SCSs have been proposed in various systems [57–73]. Recently, the generation of magnonic SCSs via magnon-photon entanglement [73] has been proposed. A pulsed optomagnonic

*dllgzfy@126.com

†lichong@dlut.edu.cn

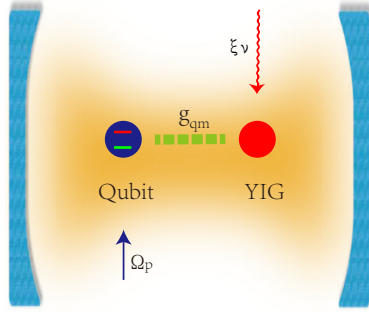


FIG. 1. Schematic of a driven hybrid ferromagnet-superconductor quantum model. The magnon is driven by a Floquet drive (red wavy arrow), while the superconducting qubit is driven by a classical microwave drive (blue straight arrow).

coupling scheme is employed to prepare the entanglement between the photon and the magnon. Single-photon operations are performed and a projective measurement is applied on the optical mode, and the magnon collapses to the SOCS or SECS.

Based on the above work, we propose an approach for generating adjustable magnonic SCSs in hybrid ferromagnet-superconductor systems. The frequency detuning between the cavity and the magnon is modulated by a low-frequency Floquet drive strength. As a result, not only can the cat state size $|\alpha|^2$ be adjusted by the Floquet drive strength, but also the fidelities of the cat states are affected by the Floquet drive strength when we consider the dissipations of the superconducting qubit and the magnon. Consequently, the generated SCSs can have a high fidelity and a large enough cat state size to be used for quantum computing. The advantages of our method are that only a cosinusoidal driving on the magnon and a classical microwave drive on the qubit are used, which can significantly improve the fidelity of SECS, and the parameters chosen in our scheme are all accessible in the state-of-the-art experimental techniques.

II. MODEL AND HAMILTONIAN

The system is shown in Fig. 1. A YIG sphere and a superconducting qubit are placed in a microwave cavity with a Floquet drive and a classical microwave drive. The total Hamiltonian of the driven hybrid ferromagnet-superconductor system reads

$$H_{\text{tot}} = \omega_c c^\dagger c + \frac{1}{2} \omega_q \sigma_z + \omega_m(t) m^\dagger m + g_q (c \sigma_+ + c^\dagger \sigma_-) + g_m (c m^\dagger + c^\dagger m) + \Omega_p (\sigma_+ e^{-i\omega_p t} + \sigma_- e^{i\omega_p t}), \quad (1)$$

with

$$\omega_m(t) = \omega_m + \xi v \cos(vt), \quad (2)$$

where $\sigma_z = |e\rangle\langle e| - |g\rangle\langle g|$ is the Pauli operator with the ground and excited state of the superconducting qubit $|g\rangle$ and $|e\rangle$; c^\dagger (c), m^\dagger (m), and σ_+ (σ_-) are the creation (annihilation) operators of the cavity, the magnon, and the superconducting qubit with the respective transition frequencies ω_c , ω_m , and ω_q ; $\omega_c c^\dagger c$, $\frac{1}{2} \omega_q \sigma_z$, and $\omega_m m^\dagger m$ are the free Hamiltonians of the cavity, the superconducting qubit, and the magnon, respectively; the fourth (fifth) term in Eq. (1) is the interac-

tion Hamiltonian between the cavity and the superconducting qubit (magnon) with coupling strength g_q (g_m); the last term in Eq. (1) is the interaction yielded by a classical microwave field with strength Ω_p and frequency ω_p . A Floquet periodic drive with a Floquet drive strength ξv and frequency v applied to the magnon and the Floquet term of the Hamiltonian is $\xi v m^\dagger m \cos(vt)$. The classical microwave drive is resonant with the superconducting qubit.

We define $\epsilon(t) = \xi \sin(vt)$ as a dynamical phase. Under the unitary operating $U_1 = \exp\{i\omega_c c^\dagger c t + i\omega_q \sigma_z t/2 + i[\omega_m t + \epsilon(t)] m^\dagger m\}$, the Hamiltonian H_{tot} becomes

$$H_1 = g_q (c^\dagger \sigma_- e^{-i\Delta t} + c \sigma_+ e^{i\Delta t}) + \Omega_p (\sigma_+ + \sigma_-) + g_m (c^\dagger m e^{-i\Delta t} e^{-i\epsilon(t)} + c m^\dagger e^{i\Delta t} e^{i\epsilon(t)}), \quad (3)$$

where $\Delta = \omega_q - \omega_c$ is the frequency detuning between the superconducting qubit and the cavity. Under the low-frequency Floquet drive modulation regime $v/\Delta \ll 1$, one can obtain $\sin(vt) \approx vt$ when we consider a time period $vt \ll 1$. We define the detuning modulated by the Floquet driving strength as $\Delta' = \Delta + \xi v$. When the large detuning condition $\Delta \gg g_q$ is satisfied, we obtain $\Delta' \gg g_m$. For a weak damping rate cavity $\gamma_c/g_q \leq 0.01$ where γ_c is the dissipation coefficient of the cavity mode, we can therefore adiabatically eliminate the cavity mode. Under the large detuning condition, the effective Hamiltonian of Eq. (3) reads

$$H_2 = g_{\text{eff}} (m \sigma_+ e^{-i\xi v t} + m^\dagger \sigma_- e^{i\xi v t}) + \Omega_p (\sigma_+ + \sigma_-), \quad (4)$$

where $g_{\text{eff}} = g_q g_m (\Delta + \Delta')/\Delta \Delta'$ is the effective coupling between the superconducting qubit and the magnon.

In the rotating frame $U_2 = e^{i\Omega_p \sigma_x t}$, the Hamiltonian in Eq. (4) can be written as

$$H_3 = g_{\text{eff}} \left\{ \left[\frac{\sigma_x}{2} + \frac{1}{2} (-\sigma_z + i\sigma_y) e^{2i\Omega_p t} + \frac{1}{2} (i\sigma_y + \sigma_z) e^{-2i\Omega_p t} \right] m e^{-i\xi v t} + \text{H.c.} \right\}, \quad (5)$$

where $\sigma_x = |e\rangle\langle g| + |g\rangle\langle e|$ and $\sigma_y = -i(|e\rangle\langle g| - |g\rangle\langle e|)$ are the Pauli matrices. In the strong-drive case $2\Omega_p \gg g_{\text{eff}}/2$, ξv , the rapidly oscillating terms of Eq. (5) can be neglected by the rotating-wave approximation (RWA), so that the Hamiltonian H_3 can be written in the form as

$$H_{3\text{eff}} = g_{\text{eff}} \sigma_x (m e^{-i\xi v t} + m^\dagger e^{i\xi v t})/2. \quad (6)$$

The Hamiltonian describes the coherent coupling between the magnon and a superconducting qubit in our system.

III. GENERATION OF THE CAT STATES

By using the Magnus expansion [74], we can express the unitary evolution operator associated with $H_{3\text{eff}}$ as

$$U(t) = \exp[i\theta(t)] \exp[\sigma_x [\eta(t) m^\dagger - \eta(t)^* m]], \quad (7)$$

where $\theta(t) = (g/\xi v)^2 [\xi v t - \sin(\xi v t)]$ is the global phase factor and $\eta(t) = (g/\xi v)(1 - e^{i\xi v t})$ is the displacement amplitude of the magnon. In the original representation, the state writes as $|\psi(t)\rangle$. The state in the rotating framework representation is defined by $|\phi(t)\rangle$. We have $|\psi(t)\rangle = V(t)|\phi(t)\rangle$

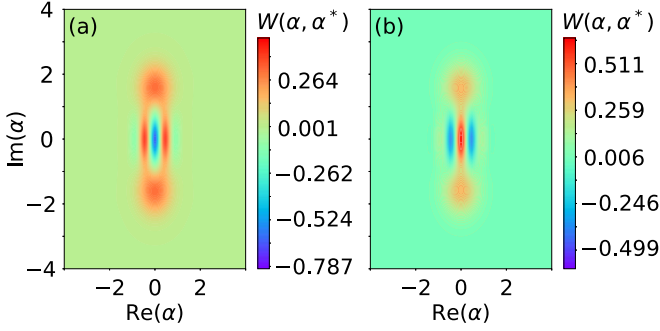


FIG. 2. Plots of the Wigner distributions of ideal (a) odd and (b) even magnonic cat states. The coherent amplitude $|\alpha|$ is 1.589. Other parameters are $t = 70$ ns, $\xi v/2\pi = 0.01$ MHz, $v/2\pi = 10$ MHz.

with $V(t) = U_1^\dagger U_2^\dagger$. When $t = 0$, one can obtain that $|\psi(0)\rangle = |\phi(0)\rangle$.

When the superconducting qubit is in the eigenstates $|\uparrow\rangle$ and $|\downarrow\rangle$ of the σ_x operator where $|\uparrow\rangle = (|e\rangle + |g\rangle)/\sqrt{2}$ and $|\downarrow\rangle = (|e\rangle - |g\rangle)/\sqrt{2}$, we have $\sigma_x|\uparrow\rangle = |\uparrow\rangle$ and $\sigma_x|\downarrow\rangle = -|\downarrow\rangle$ and the corresponding displacement operators of the magnon are in opposite directions. Therefore, the initial state of the whole system can be considered as $|\phi(0)\rangle = |0\rangle \otimes |g\rangle$ where $|0\rangle$ is the ground state of the magnon. Therefore, the system's state at time t is obtained under the unitary evolution operator $U(t)$ as

$$|\phi(t)\rangle = \frac{1}{\sqrt{2}}(|\alpha\rangle - |-\alpha\rangle)|e\rangle + \frac{1}{\sqrt{2}}(|\alpha\rangle + |-\alpha\rangle)|g\rangle. \quad (8)$$

where $|\alpha\rangle$ is the coherent state of the magnon with the complex variable

$$\alpha = (g/\xi v)(1 - e^{i\xi vt}). \quad (9)$$

The coherent amplitude $|\alpha|$ is zero when $t = 2n\pi/\xi v$ for the natural numbers n . The entanglement disappears as the superconducting qubit and the magnon decouple.

IV. FIDELITIES AND WIGNER FUNCTION

The Wigner function represents a phase-space quasiprobability distribution. We will calculate the Wigner function to observe the quantum features of the generated SCSs. For the determined magnon density matrix ρ_m , the corresponding Wigner function is defined as

$$W(\alpha, \alpha^*) = \frac{1}{\pi^2} \int e^{\eta^* \alpha - \eta \alpha^*} \chi(\eta) d^2 \eta, \quad (10)$$

with the characteristic function $\chi(\eta) = \text{Tr}\{\rho_m e^{\eta \hat{a}^\dagger - \eta^* \hat{a}}\}$. Figure 2 shows that the symcenter of the SOCS is negative, in contrast to the positive symcenter of the SECS. The Floquet driving strength $\xi v/2\pi = 0.01$ MHz and the measurement time $t = 70$ ns. The coherent amplitude $|\alpha|$ is 1.589. The superposition of two coherent states with opposite phases results in the interference phenomena and a negative value of the Wigner function performs the quantum characteristics of the magnon.

We will examine the effect of how the dissipation acts on the fidelity and the Wigner function. After taking into account the damping caused by the system-bath coupling, the driven

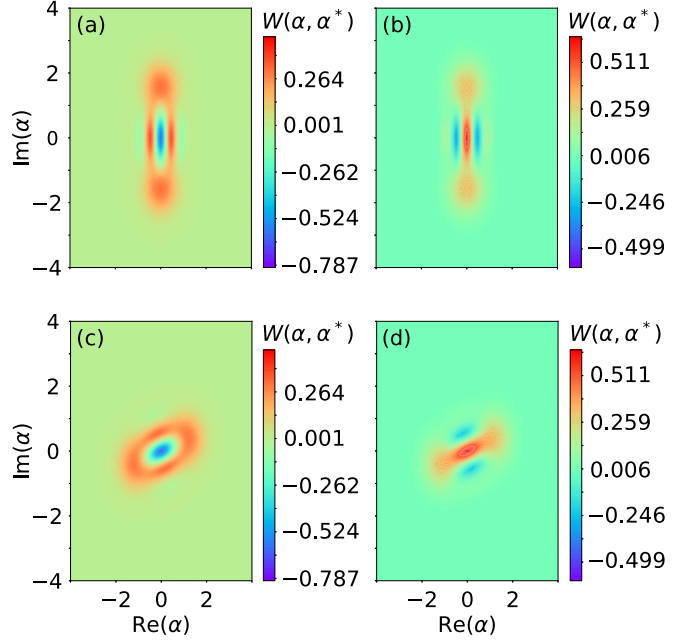


FIG. 3. Wigner functions of transient magnonic cat states with damping rate $\gamma_q = g_q/500$ and $\kappa_m = g_m/500$. Floquet periodic drive strength $\xi v/2\pi = 0.01$ MHz [(a), (b)] and 5.65 MHz [(c), (d)]. The coherent amplitude $|\alpha| = 1.589$ [(a), (b)] and 1.205 [(c), (d)]. Other parameters are the same as in Fig. 2.

hybrid ferromagnet-superconductor system is governed by the Lindblad quantum master equation

$$\begin{aligned} \frac{\partial \rho}{\partial t} = & -i[H_{\text{3eff}}, \rho] + \frac{\kappa_m}{2}(n_{\text{th}} + 1)\mathcal{L}_m[\rho] \\ & + \frac{\kappa_m}{2}n_{\text{th}}\mathcal{L}_{m^\dagger}[\rho] + \frac{\gamma_q}{2}\mathcal{L}_{\sigma_-}[\rho], \end{aligned} \quad (11)$$

where ρ is the density matrix of the system; $\mathcal{L}_m[\rho] = 2m\rho m^\dagger - m^\dagger m\rho - \rho m^\dagger m$ and $\mathcal{L}_{\sigma_-}[\rho] = 2\sigma_- \rho \sigma_+ - \sigma_+ \sigma_- \rho - \rho \sigma_+ \sigma_-$ are the Lindblad superoperators for operator m and σ_- ; $n_{\text{th}} = [e^{w_m/K_B T} - 1]^{-1}$ is the average number of the magnon at temperature T with Boltzmann constant K_B ; κ_m and γ_q are the damping rates of the magnon and the superconducting qubit. A pure state $|\phi(0)\rangle$ is transformed into a mixed state ρ as it evolves over time. By taking a partial trace of the density operator of a subsystem of a composite quantum system, one can obtain the density operator of the subsystem as well. The mixed state of the magnon is the reduced density matrix $\rho_m = \text{Tr}_q(\rho)$. In addition, the master equation (11) can be solved numerically by QUTIP [75,76]. Fidelity represents the difference between two states, which is defined as

$$F = \text{Tr}(\rho_m \rho_0), \quad (12)$$

where $\rho_0 = \text{Tr}_q|\phi(t)\rangle\langle\phi(t)|$ is the density matrix of the magnon without the dissipations.

We consider the superconducting qubit and the magnon damping rate $\gamma_q = g_q/500$ and $\kappa_q = g_m/500$. When the Floquet periodic drive strengths $\xi v/2\pi = 0.01$ MHz are taken into account, we plot the Wigner distribution of odd [Fig. 3(a)] and even [Fig. 3(b)] cat states. The coherent amplitude $|\alpha| = 1.589$ is obtained. In addition, the fidelities of SOCS

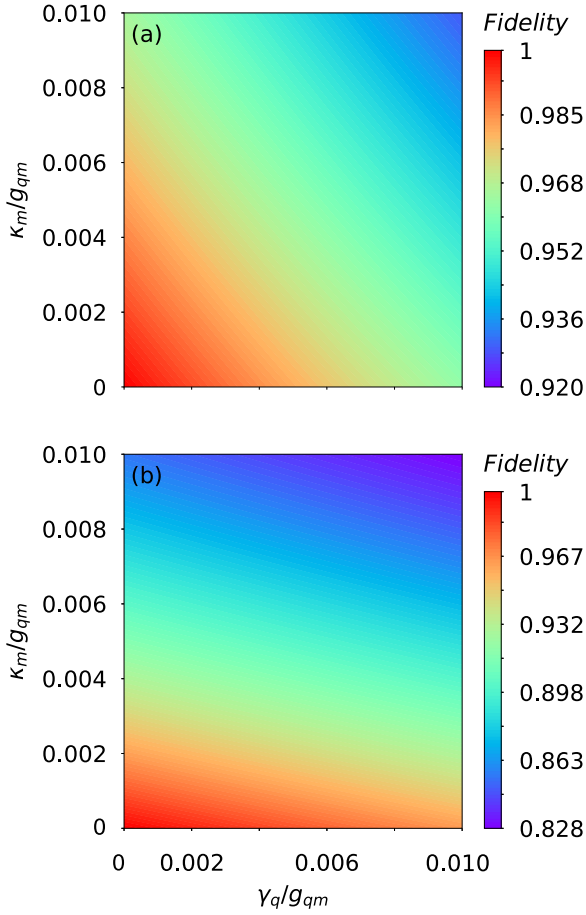


FIG. 4. Fidelities of (a) odd and (b) even SCSs are plotted with dimensionless parameters γ_q/g_{qm} and κ_m/g_{qm} . The parameters used are $t = 70$ ns, $\xi v/2\pi = 0.01$ MHz, and $v/2\pi = 10$ MHz.

and SECS are $F_{\text{odd}} = 0.985$ and $F_{\text{even}} = 0.956$. Then we set $\xi v/2\pi = 5.65$ MHz, and in this case, $|\alpha| = 1.200$, $F_{\text{odd}} = 0.981$, and $F_{\text{even}} = 0.967$. Because α is time dependent, therefore the SCSs we generate are also correlated with the measurement time t . Additionally, if only the measurement time for the superconducting qubit is changed, the size of $|\alpha|$ can reach to 2.043 with $t = 90$ ns and $\xi v/2\pi = 0.01$ MHz. The fidelities F_{odd} and F_{even} are 0.966 and 0.931 with corresponding damping rates $\gamma_q = g_q/500$ and $\kappa_q = g_m/500$. As the coherent amplitude $|\alpha|$ increases, the two coherent states become more distant and are more easily distinguishable in phase space. A large enough $|\alpha|$ means our scheme can be utilized in continuous-variable quantum computing or resources for quantum error correction coding [77–82]. By adjusting the Floquet drive strength $\xi v/2\pi = 5.90$ MHz, F_{odd} is 0.960 and F_{even} is 0.954 with $|\alpha| = 1.207$. Based on the above results, as $\xi v/2\pi$ increases gradually, the cat state rotates clockwise in phase space and $|\alpha|$ decreases. As the damping rates γ_q and κ_m increase, the Wigner functions decrease gradually, which means that the interference phenomena become weaker and the SCSs eventually become two completely separated coherent states. The transition from quantum to classical is marked by the disappearance of the magnon interference phenomena.

We plot the fidelity in Fig. 4 to observe the effects of dissipation with $t = 70$ ns and $\xi v/2\pi = 0.01$ MHz. When

the damping rates are $\gamma_q = g_q/100$, $\kappa_m = g_m/100$, it can be found that $F_{\text{odd}} = 0.929$ and F_{even} is 0.828. The impacts of dissipation on odd and even SCSs are different. F_{odd} decreases slower than F_{even} under the affect of κ_m . It is in contrast to a little faster under dissipation of the superconducting qubit γ_q . With the increase of the damping rates γ_q and κ_m , the fidelities and the Wigner functions attenuate gradually, which means that the macroscopic quantum coherence will be hurt by the dissipations of the superconducting qubit and the magnon.

V. DISCUSSIONS AND CONCLUSIONS

Due to the interaction between a superconducting qubit and the cavity mode TE_{102} , the frequency of a superconducting qubit $\omega_q/2\pi$ is shifted by -71 MHz (Lamb shift) from $\omega_{q,\text{bare}}/2\pi$ and the frequency of the cavity mode $\omega_c/2\pi$ is subject to a $+68$ MHz shift [13]. The renormalized frequencies of the superconducting qubit $\omega_q/2\pi$ and the cavity $\omega_c/2\pi$ are 8.136 and 8.488 GHz and the frequency of the magnon ω_m is 8.136 GHz [13]. The cavity-magnon (cavity-qubit) coupling strength g_m (g_q) is 21 MHz (121 MHz) [13]. On the other hand, with the application of a rotating-wave approximation (RWA), the rapidly oscillating anti-Jaynes-Cummings terms $g_q(c^\dagger\sigma_+ + c\sigma_-)$ and $g_m(c^\dagger m^\dagger + cm)$ have been neglected. In the derivation of Eq. (6), we apply the RWA to neglect the rapidly oscillating terms $\frac{1}{2}(-\sigma_z + i\sigma_y)e^{2i\Omega_p t} + \frac{1}{2}(i\sigma_y + \sigma_z)e^{-2i\Omega_p t}$ [83]. Therefore, the validity of the effective Hamiltonian can be ensured when the classical microwave drive strength $\Omega_p/2\pi \approx 10g_{\text{eff}}$ is around 70 MHz. In our scheme, the time required to generate the cat states is roughly 70 ns. As a result, when the frequency of the Floquet drive is within 10 MHz, we can get $\sin(\nu t) \approx \nu t$. When the

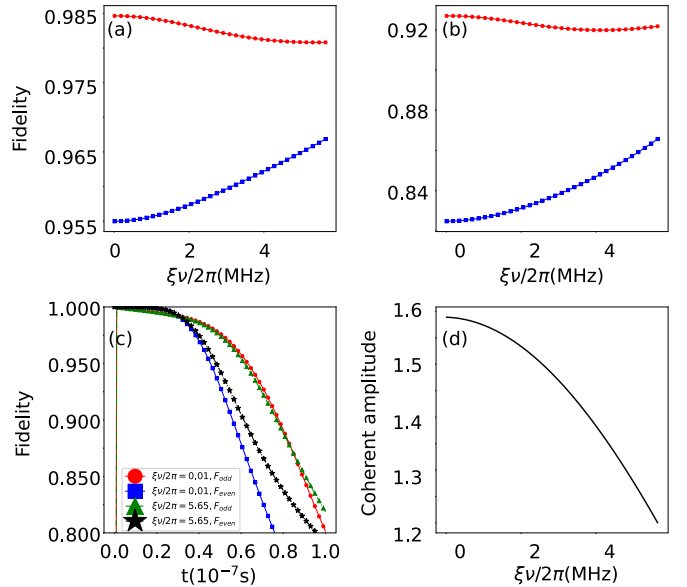


FIG. 5. The fidelities of SOCS (red circle curve) and SECS (blue square curve) vs ξv for different cases: (a) $\gamma_q/g_q = 1/500$, $\kappa_m/g_m = 1/500$, and (b) $\gamma_q/g_q = 1/100$, $\kappa_m/g_m = 1/100$. Other parameters are $t = 70$ ns and $v/2\pi = 10$ MHz. (c) The fidelities vs t with parameters $\xi v/2\pi = 0.01$ and 5.65 MHz with $\gamma_q/g_q = 1/100$, $\kappa_m/g_m = 1/100$, and $v/2\pi = 10$ MHz. (d) Coherent amplitude $|\alpha|$ vs Floquet drive strength $\xi v/2\pi$.

temperature T is around 10 mK [13], $k_B T \ll \omega_m, \omega_q$ can be satisfied. Therefore, the initial states of the superconducting qubit and the magnon are nearly in their ground states $|g\rangle$ and $|0\rangle$, respectively. As a result, the transition from the state $|e\rangle$ to $|g\rangle$ indicates the transition from the ground state of the magnon to a single-magnon state. In experiments, the Floquet driving in the magnon-cavity system is realized by the frequency modulation of the magnon through a small coil looped around the YIG sphere [84,85]. The coil is aligned along the bias field direction.

Furthermore, we plot the variation of fidelity with different parameters in Fig. 5. In Figs. 5(a) and 5(b), we plot the fidelities as functions of the Floquet drive strength $\xi\nu$. When the time is 70 ns, the fidelity of the SOCS improves significantly as the drive strength increases. We plot the variation of fidelities over time with a different Floquet drive strength in Fig. 5(c) with the dissipation $\gamma_q/g_q = 1/100$ and $\kappa_m/g_m = 1/100$. The red circle curve intersects the green triangle curve at 84 ns and this indicates that the fidelity of the odd cat state with a strong Floquet will be stronger than a weak drive after 84 ns. Therefore, both F_{odd} and F_{even} can be enhanced by the Floquet drive strength. Furthermore, we find the coherent amplitude decreases as the Floquet drive strength increases in Fig. 5(d). Therefore, we always need to keep the

coherent amplitude $|\alpha| > 1.2$ when we enhance the Floquet drive strength.

In conclusion, we propose a scheme to generate adjustable SCSs in the hybrid ferromagnet-superconductor system. The scheme is based on the coherent coupling between the magnon and the superconducting qubit by the virtual excitation of the cavity. Meanwhile, we present a detailed analysis of the Wigner functions and the fidelities in an open system. The fidelities of the prepared SCSs can be adjusted by the strength of the Floquet drive and the timing of the measurement for the superconducting qubit. A larger cat state can be obtained when the Floquet drive strength is decreased. On the other hand, the cat state size $|\alpha|^2$ increases while the fidelities decrease. Therefore, when an appropriate Floquet drive strength and measurement time for the superconducting qubit are selected, adjustable SCSs with a high fidelity and large size can be obtained.

ACKNOWLEDGMENTS

We thank Wenlin Li, Yexiong Zeng, and Chongsong Zhao for constructive discussions. The work was funded by the National Natural Science Foundation of China (Grant No. 12274053).

-
- [1] Z.-L. Xiang, S. Ashhab, J. Q. You, and F. Nori, Hybrid quantum circuits: Superconducting circuits interacting with other quantum systems, *Rev. Mod. Phys.* **85**, 623 (2013).
 - [2] G. Kurizki, P. Bertet, Y. Kubo, K. Mølmer, D. Petrosyan, P. Rabl, and J. Schmiedmayer, Quantum technologies with hybrid systems, *Proc. Natl. Acad. Sci. USA* **112**, 3866 (2015).
 - [3] M. Wallquist, K. Hammerer, P. Rabl, M. Lukin, and P. Zoller, Hybrid quantum devices and quantum engineering, *Phys. Scr.*, **T 137**, 014001 (2009).
 - [4] M. H. Devoret and R. J. Schoelkopf, Superconducting circuits for quantum information: An outlook, *Science* **339**, 1169 (2013).
 - [5] J. Q. You and F. Nori, Superconducting circuits and quantum information, *Phys. Today* **58**(11), 42 (2005).
 - [6] J. Q. You, X. Hu, S. Ashhab, and F. Nori, Low-decoherence flux qubit, *Phys. Rev. B* **75**, 140515 (2007).
 - [7] J. Koch, T. M. Yu, J. Gambetta, A. A. Houck, D. I. Schuster, J. Majer, A. Blais, M. H. Devoret, S. M. Girvin, and R. J. Schoelkopf, Charge-insensitive qubit design derived from the Cooper pair box, *Phys. Rev. A* **76**, 042319 (2007).
 - [8] R. Barends, J. Kelly, A. Megrant, A. Veitia, D. Sank, E. Jeffrey, T. C. White, J. Mutus, A. G. Fowler, B. Campbell, Y. Chen, Z. Chen, B. Chiaro, A. Dunsworth, C. Neill, P. O'Malley, P. Roushan, A. Vainsencher, J. Wenner, A. N. Korotkov *et al.*, Superconducting quantum circuits at the surface code threshold for fault tolerance, *Nature (London)* **508**, 500 (2014).
 - [9] J. Clarke and F. K. Wilhelm, Superconducting quantum bits, *Nature (London)* **453**, 1031 (2008).
 - [10] J. Q. You and F. Nori, Atomic physics and quantum optics using superconducting circuits, *Nature (London)* **474**, 589 (2011).
 - [11] I. Buluta, S. Ashhab, and F. Nori, Natural and artificial atoms for quantum computation, *Rep. Prog. Phys.* **74**, 104401 (2011).
 - [12] X. Gu, A. F. Kockum, A. Miranowicz, Y. xi Liu, and F. Nori, Microwave photonics with superconducting quantum circuits, *Phys. Rep.* **718-719**, 1 (2017).
 - [13] Y. Tabuchi, S. Ishino, A. Noguchi, T. Ishikawa, R. Yamazaki, K. Usami, and Y. Nakamura, Coherent coupling between a ferromagnetic magnon and a superconducting qubit, *Science* **349**, 405 (2015).
 - [14] F.-Y. Zhang, W.-B. Yan, and C.-P. Yang, Generalized coupling system between a superconducting qubit and two nanomechanical resonators, *Phys. Rev. A* **98**, 042331 (2018).
 - [15] H. Huebl, C. W. Zollitsch, J. Lotze, F. Hocke, M. Greifenstein, A. Marx, R. Gross, and S. T. B. Goennenwein, High Cooperativity in Coupled Microwave Resonator Ferrimagnetic Insulator Hybrids, *Phys. Rev. Lett.* **111**, 127003 (2013).
 - [16] M. Goryachev, W. G. Farr, D. L. Creedon, Y. Fan, M. Kostylev, and M. E. Tobar, High-Cooperativity Cavity QED with Magnons at Microwave Frequencies, *Phys. Rev. Appl.* **2**, 054002 (2014).
 - [17] X. Zhang, C.-L. Zou, L. Jiang, and H. X. Tang, Strongly Coupled Magnons and Cavity Microwave Photons, *Phys. Rev. Lett.* **113**, 156401 (2014).
 - [18] K. Uchida, J. Xiao, H. Adachi, J. Ohe, S. Takahashi, J. Ieda, T. Ota, Y. Kajiwara, H. Umezawa, H. Kawai, G. E. W. Bauer, S. Maekawa, and E. Saitoh, Spin seebeck insulator, *Nat. Mater.* **9**, 894 (2010).
 - [19] Y. Kajiwara, K. Harii, S. Takahashi, J. Ohe, K. Uchida, M. Mizuguchi, H. Umezawa, H. Kawai, K. Ando, K. Takanashi, S. Maekawa, and E. Saitoh, Transmission of electrical signals by spin-wave interconversion in a magnetic insulator, *Nature (London)* **464**, 262 (2010).
 - [20] Y. Tabuchi, S. Ishino, T. Ishikawa, R. Yamazaki, K. Usami, and Y. Nakamura, Hybridizing Ferromagnetic Magnons and

- Microwave Photons in the Quantum Limit, *Phys. Rev. Lett.* **113**, 083603 (2014).
- [21] H. Yuan, Y. Cao, A. Kamra, R. A. Duine, and P. Yan, Quantum magnonics: When magnon spintronics meets quantum information science, *Phys. Rep.* **965**, 1 (2022).
- [22] R. Hisatomi, A. Osada, Y. Tabuchi, T. Ishikawa, A. Noguchi, R. Yamazaki, K. Usami, and Y. Nakamura, Bidirectional conversion between microwave and light via ferromagnetic magnons, *Phys. Rev. B* **93**, 174427 (2016).
- [23] A. Osada, R. Hisatomi, A. Noguchi, Y. Tabuchi, R. Yamazaki, K. Usami, M. Sadgrove, R. Yalla, M. Nomura, and Y. Nakamura, Cavity Optomagnonics with Spin-Orbit Coupled Photons, *Phys. Rev. Lett.* **116**, 223601 (2016).
- [24] X. Zhang, N. Zhu, C.-L. Zou, and H. X. Tang, Optomagnonic Whispering Gallery Microresonators, *Phys. Rev. Lett.* **117**, 123605 (2016).
- [25] J. A. Haigh, A. Nunnenkamp, A. J. Ramsay, and A. J. Ferguson, Triple-Resonant Brillouin Light Scattering in Magneto-Optical Cavities, *Phys. Rev. Lett.* **117**, 133602 (2016).
- [26] S. Viola Kusminskiy, H. X. Tang, and F. Marquardt, Coupled spin-light dynamics in cavity optomagnonics, *Phys. Rev. A* **94**, 033821 (2016).
- [27] S. Sharma, Y. M. Blanter, and G. E. W. Bauer, Light scattering by magnons in whispering gallery mode cavities, *Phys. Rev. B* **96**, 094412 (2017).
- [28] A. Osada, A. Gloppe, Y. Nakamura, and K. Usami, Orbital angular momentum conservation in Brillouin light scattering within a ferromagnetic sphere, *New J. Phys.* **20**, 103018 (2018).
- [29] A. Osada, A. Gloppe, R. Hisatomi, A. Noguchi, R. Yamazaki, M. Nomura, Y. Nakamura, and K. Usami, Brillouin Light Scattering by Magnetic Quasivortices in Cavity Optomagnonics, *Phys. Rev. Lett.* **120**, 133602 (2018).
- [30] C. Zhao, Z. Yang, R. Peng, J. Yang, C. Li, and L. Zhou, Dissipative-Coupling-Induced Transparency and High-Order Sidebands with Kerr Nonlinearity in a Cavity-Magnonics System, *Phys. Rev. Appl.* **18**, 044074 (2022).
- [31] Y. Tabuchi, S. Ishino, A. Noguchi, T. Ishikawa, R. Yamazaki, K. Usami, and Y. Nakamura, Quantum magnonics: The magnon meets the superconducting qubit, *C. R. Phys.* **17**, 729 (2016).
- [32] Y.-P. Wang, G.-Q. Zhang, D. Zhang, T.-F. Li, C.-M. Hu, and J. Q. You, Bistability of Cavity Magnon Polaritons, *Phys. Rev. Lett.* **120**, 057202 (2018).
- [33] F.-Y. Zhang, Q.-C. Flu, and C.-P. Yang, Non-Hermitian shortcut to adiabaticity in Floquet cavity electromagnonics, *Phys. Rev. A* **106**, 012609 (2022).
- [34] D. Zhang, X.-Q. Luo, Y.-P. Wang, T.-F. Li, and J. Q. You, Observation of the exceptional point in cavity magnon-polaritons, *Nat. Commun.* **8**, 1368 (2017).
- [35] Y.-P. Wang, G.-Q. Zhang, D. Zhang, X.-Q. Luo, W. Xiong, S.-P. Wang, T.-F. Li, C.-M. Hu, and J. Q. You, Magnon Kerr effect in a strongly coupled cavity-magnon system, *Phys. Rev. B* **94**, 224410 (2016).
- [36] Z.-B. Yang, W.-J. Wu, J. Li, Y.-P. Wang, and J. Q. You, Steady-entangled-state generation via the cross-Kerr effect in a ferrimagnetic crystal, *Phys. Rev. A* **106**, 012419 (2022).
- [37] R.-C. Shen, J. Li, Z.-Y. Fan, Y.-P. Wang, and J. You, Mechanical Bistability in Kerr-Modified Cavity Magnomechanics, *Phys. Rev. Lett.* **129**, 123601 (2022).
- [38] J. W. Rao, P. C. Xu, Y. S. Gui, Y. P. Wang, Y. Yang, B. Yao, J. Dietrich, G. E. Bridges, X. L. Fan, D. S. Xue, and C.-M. Hu, Interferometric control of magnon-induced nearly perfect absorption in cavity magnonics, *Nat. Commun.* **12**, 1933 (2021).
- [39] Y. Li, T. Polakovic, Y.-L. Wang, J. Xu, S. Lendinez, Z. Zhang, J. Ding, T. Khaire, H. Saglam, R. Divan, J. Pearson, W.-K. Kwok, Z. Xiao, V. Novosad, A. Hoffmann, and W. Zhang, Strong Coupling between Magnons and Microwave Photons in On-Chip Ferromagnet-Superconductor Thin-Film Devices, *Phys. Rev. Lett.* **123**, 107701 (2019).
- [40] J. Li, S.-Y. Zhu, and G. S. Agarwal, Magnon-Photon-Phonon Entanglement in Cavity Magnomechanics, *Phys. Rev. Lett.* **121**, 203601 (2018).
- [41] D. Xu, X.-K. Gu, H.-K. Li, Y.-C. Weng, Y.-P. Wang, J. Li, H. Wang, S.-Y. Zhu, and J. You, Quantum control of a single magnon in a macroscopic spin system, *arXiv:2211.06644*.
- [42] S.-f. Qi and J. Jing, Generation of Bell and Greenberger-Horne-Zeilinger states from a hybrid qubit-photon-magnon system, *Phys. Rev. A* **105**, 022624 (2022).
- [43] Z.-X. Liu, H. Xiong, and Y. Wu, Magnon blockade in a hybrid ferromagnet-superconductor quantum system, *Phys. Rev. B* **100**, 134421 (2019).
- [44] J.-k. Xie, S.-l. Ma, and F.-l. Li, Quantum-interference-enhanced magnon blockade in an yttrium-iron-garnet sphere coupled to superconducting circuits, *Phys. Rev. A* **101**, 042331 (2020).
- [45] E. Schrödinger, Die gegenwärtige Situation in der Quantenmechanik, *Naturwissenschaften* **23**, 823 (1935).
- [46] Y. Xia and G. Guo, Nonclassical properties of even and odd coherent states, *Phys. Lett. A* **136**, 281 (1989).
- [47] J. Janszky and A. V. Vinogradov, Squeezing Via One-Dimensional Distribution of Coherent States, *Phys. Rev. Lett.* **64**, 2771 (1990).
- [48] J. Janszky, P. Domokos, and P. Adam, Coherent states on a circle and quantum interference, *Phys. Rev. A* **48**, 2213 (1993).
- [49] J. Janszky, P. Domokos, S. Szabó, and P. Adam, Quantum-state engineering via discrete coherent-state superpositions, *Phys. Rev. A* **51**, 4191 (1995).
- [50] M. O. Scully and M. S. Zubairy, *Quantum Optics* (Cambridge University Press, Cambridge, UK, 1999).
- [51] B. C. Sanders, Entangled coherent states, *Phys. Rev. A* **45**, 6811 (1992).
- [52] J. Wenger, M. Hafezi, F. Grosshans, R. Tualle-Brouiri, and P. Grangier, Maximal violation of Bell inequalities using continuous-variable measurements, *Phys. Rev. A* **67**, 012105 (2003).
- [53] H. Jeong, W. Son, M. S. Kim, D. Ahn, and C. Brukner, Quantum nonlocality test for continuous-variable states with dichotomic observables, *Phys. Rev. A* **67**, 012106 (2003).
- [54] M. Stobińska, H. Jeong, and T. C. Ralph, Violation of Bell's inequality using classical measurements and nonlinear local operations, *Phys. Rev. A* **75**, 052105 (2007).
- [55] M. Brune, E. Hagley, J. Dreyer, X. Maître, A. Maali, C. Wunderlich, J. M. Raimond, and S. Haroche, Observing the Progressive Decoherence of the “Meter” in a Quantum Measurement, *Phys. Rev. Lett.* **77**, 4887 (1996).
- [56] C. Monroe, D. M. Meekhof, B. E. King, and D. J. Wineland, A “Schrödinger cat” superposition state of an atom, *Science* **272**, 1131 (1996).
- [57] S. Bose, K. Jacobs, and P. L. Knight, Preparation of nonclassical states in cavities with a moving mirror, *Phys. Rev. A* **56**, 4175 (1997).

- [58] B. Yurke and D. Stoler, Generating Quantum Mechanical Superpositions of Macroscopically Distinguishable States Via Amplitude Dispersion, *Phys. Rev. Lett.* **57**, 13 (1986).
- [59] B. Yurke, W. Schleich, and D. F. Walls, Quantum superpositions generated by quantum nondemolition measurements, *Phys. Rev. A* **42**, 1703 (1990).
- [60] M. Brune, S. Haroche, J. M. Raimond, L. Davidovich, and N. Zagury, Manipulation of photons in a cavity by dispersive atom-field coupling: Quantum-nondemolition measurements and generation of “Schrödinger cat” states, *Phys. Rev. A* **45**, 5193 (1992).
- [61] E. Solano, G. S. Agarwal, and H. Walther, Strong-Driving-Assisted Multipartite Entanglement in Cavity QED, *Phys. Rev. Lett.* **90**, 027903 (2003).
- [62] J. Huang, Y.-H. Liu, J.-F. Huang, and J.-Q. Liao, Generation of macroscopic entangled cat states in a longitudinally coupled cavity-QED model, *Phys. Rev. A* **101**, 043841 (2020).
- [63] Y.-H. Chen, W. Qin, X. Wang, A. Miranowicz, and F. Nori, Shortcuts to Adiabaticity for the Quantum Rabi Model: Efficient Generation of Giant Entangled Cat States via Parametric Amplification, *Phys. Rev. Lett.* **126**, 023602 (2021).
- [64] W. Qin, A. Miranowicz, H. Jing, and F. Nori, Generating Long-Lived Macroscopically Distinct Superposition States in Atomic Ensembles, *Phys. Rev. Lett.* **127**, 093602 (2021).
- [65] F.-Y. Zhang and C.-P. Yang, Generation of generalized hybrid entanglement in cavity electro-optic systems, *Quantum Sci. Technol.* **6**, 025003 (2021).
- [66] F. Zou, L.-B. Fan, J.-F. Huang, and J.-Q. Liao, Enhancement of few-photon optomechanical effects with cross-Kerr nonlinearity, *Phys. Rev. A* **99**, 043837 (2019).
- [67] D.-G. Lai, J.-Q. Liao, A. Miranowicz, and F. Nori, Noise-Tolerant Optomechanical Entanglement Via Synthetic Magnetism, *Phys. Rev. Lett.* **129**, 063602 (2022).
- [68] D.-G. Lai, J.-F. Huang, X.-L. Yin, B.-P. Hou, W. Li, D. Vitali, F. Nori, and J.-Q. Liao, Nonreciprocal ground-state cooling of multiple mechanical resonators, *Phys. Rev. A* **102**, 011502 (2020).
- [69] W. Qin, A. Miranowicz, G. Long, J. Q. You, and F. Nori, Proposal to test quantum wave-particle superposition on massive mechanical resonators, *npj Quantum Inf.* **5**, 58 (2019).
- [70] Y.-X. Zeng, J. Shen, M.-S. Ding, and C. Li, Macroscopic Schrödinger cat state swapping in optomechanical system, *Opt. Express* **28**, 9587 (2020).
- [71] B. Li, W. Qin, Y.-F. Jiao, C.-L. Zhai, X.-W. Xu, L.-M. Kuang, and H. Jing, Optomechanical Schrödinger cat states in a cavity Bose-Einstein condensate, *Fundam. Res.* **3**, 15 (2022).
- [72] C. C. Gerry, Schrödinger cat states in a Josephson junction, *Phys. Rev. B* **57**, 7474 (1998).
- [73] F.-X. Sun, S.-S. Zheng, Y. Xiao, Q. Gong, Q. He, and K. Xia, Remote Generation of Magnon Schrödinger Cat State via Magnon-Photon Entanglement, *Phys. Rev. Lett.* **127**, 087203 (2021).
- [74] J.-Q. Liao, J.-F. Huang, and L. Tian, Generation of macroscopic Schrödinger-cat states in qubit-oscillator systems, *Phys. Rev. A* **93**, 033853 (2016).
- [75] J. Johansson, P. Nation, and F. Nori, QuTiP: An open-source Python framework for the dynamics of open quantum systems, *Comput. Phys. Commun.* **183**, 1760 (2012).
- [76] J. Johansson, P. Nation, and F. Nori, QuTiP 2: A Python framework for the dynamics of open quantum systems, *Comput. Phys. Commun.* **184**, 1234 (2013).
- [77] K. Takase, J.-i. Yoshikawa, W. Asavanant, M. Endo, and A. Furusawa, Generation of optical Schrödinger cat states by generalized photon subtraction, *Phys. Rev. A* **103**, 013710 (2021).
- [78] P. T. Cochrane, G. J. Milburn, and W. J. Munro, Macroscopically distinct quantum-superposition states as a bosonic code for amplitude damping, *Phys. Rev. A* **59**, 2631 (1999).
- [79] T. C. Ralph, A. Gilchrist, G. J. Milburn, W. J. Munro, and S. Glancy, Quantum computation with optical coherent states, *Phys. Rev. A* **68**, 042319 (2003).
- [80] H. M. Vasconcelos, L. Sanz, and S. Glancy, All-optical generation of states for “Encoding a qubit in an oscillator”, *Opt. Lett.* **35**, 3261 (2010).
- [81] D. J. Weigand and B. M. Terhal, Generating grid states from Schrödinger-cat states without postselection, *Phys. Rev. A* **97**, 022341 (2018).
- [82] J. Hastrup, J. S. Neergaard-Nielsen, and U. L. Andersen, Deterministic generation of a four-component optical cat state, *Opt. Lett.* **45**, 640 (2020).
- [83] Q. Chen, W. Yang, and M. Feng, Generation of macroscopic entangled coherent states for distant ensembles of polar molecules via effective coupling to a superconducting charge qubit, *Phys. Rev. A* **86**, 045801 (2012).
- [84] J. Xu, C. Zhong, X. Han, D. Jin, L. Jiang, and X. Zhang, Floquet Cavity Electromagnonics, *Phys. Rev. Lett.* **125**, 237201 (2020).
- [85] M.-S. Ding, L. Zheng, and C. Li, Ground-state cooling of a magnomechanical resonator induced by magnetic damping, *J. Opt. Soc. Am. B* **37**, 627 (2020).